Summer 7-1-2018

Grasp Synthesis for Purposeful Fracturing of Object

Mahyar Abdeetedal
Amazon

Mehrdad Kermani Ph.D., P.Eng.
Western University, mkermani@eng.uwo.ca

Grasp Synthesis for Purposeful Fracturing of Object

Mahyar Abdeetedal, Mehrdad R. Kermani

***Abstract*—This paper deals with the problem of purposefully failing (breaking) or yielding objects by a robotic gripper. Robotic harvesting is considered as an application domain that motivates this study. A definition of a failure task is first formulated using failure theories. Next, a grasp quality measure is presented to characterize a suitable grasp configuration and systematically control the failure behavior of the object. This approach combines the failure task and the capability of the gripper for wrench insertion. The friction between the object and the gripper is used to formulate the capability of the gripper for wrench insertion. A new method inspired by the human pre-manipulation process is introduced to utilize the gripper itself as the measurement tool and obtain a friction model. The developed friction model is capable of capturing the anisotropic behavior of materials which is the case for most fruits and vegetables. The evaluation method proposed in this study is formulated as a quasistatic grasp problem and can include both fully-actuated and under-actuated grippers. The proposed approach for purposefully breaking objects is validated using experimental results. Objects with different material properties are used to prove the generality of the method. KUKA LightWeight Robot IV is used as the manipulator.**

***Index Terms*—Agricultural Robotics, Robotic Grasp, Grasp Evaluation, Friction Modeling.**

I. Introduction

Harvesting is the process of gathering ripe crops that can be described as breaking objects into two or more pieces at desired locations. This process has to be systematically controlled to permit successful application of robotic hands and grasp theories in harvesting and avoiding damage to the crop (see Fig. 1). The complete separation of an anisotropic beam such as a fruit stem or a tree branch is difficult to model, since buckling and green-stick fracture in biological beams complicate the process of snapping. Buckling and green-stick fracture result from anisotropic nature of fiber cells along radial and tangential directions. [1]. Nevertheless, we propose a grasp evaluation method to systematically study the process of failure by taking into consideration the mechanical and physical properties of the material.

Over the last four decades, significant contributions have been made in the field of robotic grasping [2], [3], [4]. As massively reported in the literature, robotic grasp encompasses a broad range of tasks from a simple pick and place to a more advanced assembly task such as circuit chips insertion. A common element among these tasks is the process of putting the object(s) together. In contrast, in robotic harvesting, the primary goal is the failure and separation of the grasped objects at a certain location [5], [6]. To the best of our knowledge, there is no investigation on grasp planning to fail or separate a grasped object purposefully. The studies that emphasize on avoiding deflection and/or slippage of the object [7], [8], [9], [10] ignore the individual effects of bending, tension, or torsion on the object which is essential for obtaining an accurate characterization of grasp task intended for object failure.

Mahyar Abdeetedal and Mehrdad R. Kermani are with Faculty of Electrical and Computer Engineering, Western University , London, Ontario, Canada mabdeete@uwo.ca, mkerman2@uwo.ca

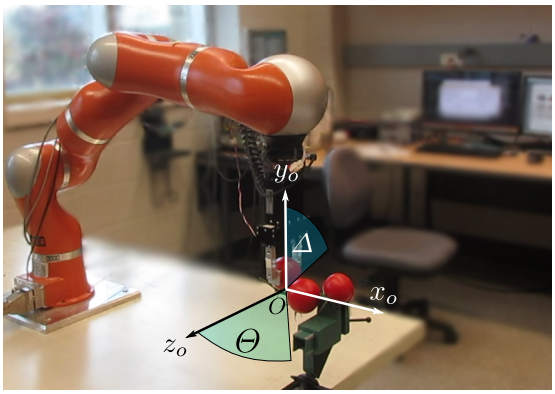

Fig. 1. Harvesting a Tomato using a robotic gripper while avoiding damage to the crop and its neighbours. Systematic object failure at the origin denoted by, O, within maximum allowable object twist denoted by Θ and maximum allowable object deflection denoted by Δ.

A grasp task can be characterized by a set of expected wrenches that the grasp must withstand during the expected manipulation process [11]. A task polytope can be defined using all these wrenches [12] known as Task Wrench Space (TWS). A TWS can be approximated by an ellipsoid [13] or a convex polytope [14]. The TWS can be used to evaluate the quality of the grasp. For instance, a well-known task-oriented grasp metric is to choose an appropriate TWS such that it is well inscribed within the grasp wrench tolerance [15]. The core of our approach involves computing the maximum force that can be applied to a grasped object so as to yield a tensile object or fracture a brittle object while optimizing contact forces and analyzing force capabilities of the gripper. To this end, we propose a new definition of the failure task using mechanical failure theories and use it to evaluate the grasp so as to measure how well the TWS conforms with the capabilities of the gripper. The grasp capability is formulated using wrench insertion capability of the gripper and the friction between the gripper and object. Friction can play a major role in grasping. To apply bending moment, tension force, and torsion torque, contact points with friction are necessary when form closure is not achievable. It is common in the literature to use Coulomb's law to model the dynamic friction force between the gripper and the object [2]. However, friction in anisotropic materials such as fruits can vary significantly and cannot be characterized using a single Coulomb's friction coefficient. Thus we consider an anisotropic friction model

and propose a method to identify the parameters of this model. The method is inspired by the approach used by humans. Several studies have demonstrated that humans adapt their exploratory movements to improve information gained through mechanical stimulus and elicit information using such interactions [16], [17], [18]. Inspired by this natural approach, we use gripper itself as a friction measurement tool during object manipulation. The contributions of this work are as follows:

- A new failure task definition is introduced to be used in grasp evaluation method. Mechanical failure theories are carefully selected for any brittle or ductile materials for accurate failure behavior prediction.
- An innovative approach to the problem of motion constraints on robotic manipulator is proposed. This problem is pervasive in robotic harvesting where either the cluster of fruits or tight working space of indoor farming demand stringent limits on the motion. An optimization method for finding a sufficient wrench for failing the object which does not require the robotic manipulator to exceed any motion limits is provided.
- A new friction identification process is proposed to measure friction parameters. The method is fast and easy to implement. It consists of moving the gripper on the object in few different directions to capture the anisotropic friction behavior of the object. The acquired frictional data are used to formulate the gripper wrench insertion capability.
- A task oriented grasp evaluation method considering the gripper capability and the optimized failure wrench is proposed. Since the gripper capability is dependent on its actuation system, both cases of the fully-actuated and under-actuated grippers are considered.

The structure of this paper is as follows: Section II provides the problem statement. Section III formally defines a failure task in the context of robotic grasping. Section IV introduces our grasp evaluation method intended for object failure. Section V evaluates the validity of the proposed approach using experimental results. Section VI provides a discussion about the significance of the findings in this paper. Section VII concludes the paper.

II. Problem Statement

In this section, grasping an object with the intention of purposefully separating it or systematically failing it is formulated. Object failure refers to the separation of the object into two or more pieces. This definition includes permanent distortion, geometric ruin, downgraded reliability, or compromised function. Failure theories predict the conditions under which solid materials fail under the action of external loads. The failure behaviour of a material is usually classified into brittle failure (fracture) or ductile failure (yield). Failure theories provide criteria which separate "failed" states from "unfailed" states.

Stress is defined as the value of force per unit area. The relative orientation of the force vector to the surface normal determines the stress as normal or shear stress when the force vector is normal or parallel to the surface, respectively. Stress can be regarded as a tensor since it obeys the standard coordinate transformation principles of tensors. A stress tensor has real eigenvalues called *principal stresses* of the stress.

Applying stress on different materials produces an amount of deformation (strain) specific to the material before failure. Figure 2 shows typical stress-strain relationship for ductile and brittle materials. This figure shows that *sufficient* amount of stress will result in permanent deformation or failure. For instance, many ductile materials including some metals, polymers, and ceramics exhibit a linear stress-strain relationship prior to failing (yield point). As the deformation increases, the material exhibits a nonlinear behavior characterized by *yielding strength* denoted by S_y and *ultimate strength* denoted by S_u. Brittle materials exhibit different stress-strain relations. For instance, many brittle materials including cast iron, glass, and stone, are characterized by the fact that fracture occurs without any noticeable prior change in the rate of strain [19]. Thus, the ultimate strength and yielding strength are the same in brittle materials.

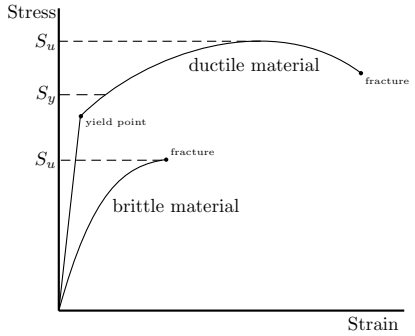

Fig. 2. A typical stress-strain diagram for ductile and brittle materials. S_y is yielding strength, and S_u is the ultimate strength. Note that the ultimate strength of brittle material is not necessarily less than the ultimate strength of ductile material.

The material information is necessary for a failing process to systematically control the set of wrenches that are inserted by the robotic gripper on the object. The set of wrenches required for the task (failure task wrench set) is generated by the forces applied at the contact points. The goal is to insert contact forces which are transformed effectively to the point of interest, i.e., the failing point. For example, to fail the object shown in Fig. 3 at point O, the wrench resulted from mapping all contact forces at $\{c_1,...,c_{n_c}\}$ to the point O must be enough for failing the object.

We combine material failure information with conventional robotic grasp formulation. A widely used assumption in robot grasp planning is the quasistatic assumption [20], [21]. This assumption requires parts to move sufficiently slowly such that all inertial effects are negligible. The Quasistatic model of the grasp is represented as,

$$w = -Gf \tag{1}$$

where $w \in R^6$ is the wrench exerted on the object by gravity and/or external sources, $G \in R^{6\times 3n_c}$ is the Grasp matrix, $f \in R^{3n_c}$ is the contact force vector, and Gf is the total

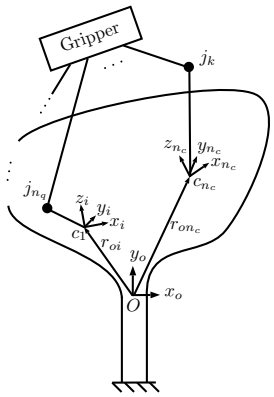

Fig. 3. Mapping between the forces and moments (with r_{oi} arm) applied at n_c contact points (c_1 to c_{n_c}) and the wrenches applied to the object at O. Also mapping between the moments of j_k applied by n_q joints of the gripper and the transmitted contact forces at n_c contact points.

wrench applied to the object by the hand. The Grasp matrix defines relevant contact forces and moments of the hand to the set of wrenches at the object's origin. In doing so, the arm vector, r_{oi} associated with each contact point is used to obtain the moments (see Fig. 3). For failing the object shown in Fig. 3, one needs to obtain the contact forces that after being mapped to the origin result in a balance with the object reaction wrenches. Additionally, internal forces must not exceed a certain amount to avoid any damage to the object. The null space of the Grasp matrix ($\mathcal{N}(G)$) represents a subspace containing internal forces. These internal forces result in wrench intensity but not the object motion. It can be easily shown that internal forces are controllable by joint actions if and only if $\mathcal{N}(G) \cap \mathcal{N}(J^T) = 0$ where J is the Jacobian matrix of the hand.

A general solution of (1) represents contact forces that are mapped to the origin and result in a balance with the object reaction wrenches, i.e.,

$$f = -G^{+}w + \mathrm{A}\xi \tag{2}$$

where G^{+} is assumed to be the right inverse of Grasp matrix, and $\mathrm{A} \in R^{3n_c \times g}$ is a matrix whose columns span the subspace of $\mathcal{N}(G)$, with $\mathcal{N}(J^T)$ excluded, and $\xi \in R^g$ is a free g-vector which parametrizes the homogeneous solution. The homogeneous part can be used for controlling the amount of squeezing of the object to avoid possible damage. This formulation represents a robotic hand which is locked around an object, e.g., a fruit to be harvested. When the inertial terms are negligible due to slow motions, the hand and object can be considered as a single load attached to the end-effector of the manipulator. The contact forces are continually being adjusted according to the external wrenches, such as gravity or the wrenches exerted by the stem in the case of harvesting.

Suitable contact forces for synthesizing a successful harvesting are highly dependent on the knowledge of the friction at contact points. It is assumed that the grasp consists of any number of hard contacts with friction. In the presence of friction, the contact force used in formulating (2) can deviate from the vector pointing in the direction of the inward surface normal. Hence, contact forces can be adjusted more freely. However, friction modeling of anisotropic materials such as crops is more challenging. Most epidermal cells of the aerial parts of the higher plants, e.g., fruits and their stems are covered with cuticle membrane (CM) which is a mixture of homologous series of aliphatic [22]. This fact explains the variations of mechanical properties, as well as the frictional behavior of the biological materials. Frictional behavior can change with respect to the direction of surfaces movement as well as other factors such as relative humidity and temperature. These variations in friction become important in formulating grasp tasks considered in this work including harvesting. Unfortunately, it is very difficult, if not impossible to capture all the variations of friction. For the purpose of grasp evaluation and grasp adjustment, this paper proposes a practical method that uses the gripper itself as a pre-manipulation tool to obtain the sufficient knowledge of the necessary friction for the intended task, i.e., a failure task.

Based on Krein-Milman theorem [23], vertices of convex hull that bound the space of task wrenches can be used for defining a grasping task. To this effect, a set of extreme wrenches can be defined if the task requirements are known. For the harvesting case, the extreme wrenches are the result of the reaction forces exerted by the stem during separation. Depending on the specific reaction behavior of a biological beam, which can vary from brittle to ductile, the failure task can be defined. There are cases in harvesting that the stem acts in a ductile manner and cannot be snapped easily. Hence, we broaden the failing task formulation here to include all types of materials.

III. Failure Grasp Task Definition

In this paper, failure is defined as a brittle part being separated into two or more pieces and a ductile part becoming permanently distorted. Failure theories help mechanical designers to immune their designs from failure. These theories provide the minimum *principal stresses* which are just enough to fail the part. These theories are conservative to not allow reaching the object stress tolerance. In this paper, failure theories are used to ensure minimum effort for purposefully failing a beam. The keyword here is *minimum effort*, since for the harvesting task, it can guarantee the health of the harvested crops by avoiding bruises or squishing forces.

There are several theories for each type of material (ductile or brittle) formulating the failure behavior. A selection of these theories are made based on the following assumptions,

- A material that normally is considered as ductile fails in a ductile manner.
- All materials are considered to have equal ultimate strengths in tension and compression.
- A beam with any general profile requires less stress to fail than a virtual cylinder from the same material covering it.

The first assumption is valid when there are no cracks in the object, and manipulation temperature is higher than the *transition temperature* which prevents sudden brittle fracture of the so-called ductile material. Yielding a ductile object can

ultimately cause cracks in it [24]. Our interest in considering the ductile materials here is based on the fact that if a biological beam acts initially in a ductile manner, it can then snap in a brittle manner after yielding. The second assumption is used for the sake of simplicity even though there are rare cases in which ultimate strengths in tension and compression are unequal (e.g., magnesium alloys). The third assumption is for generalizing the target object profile. This assumption guarantees object's failure by considering a virtual cylinder that circumscribes the object's profile, requiring larger stress than the object.

A. Ductile Material

For ductile behavior, the selected criterion is the distortion-energy theory. Maximum shear stress theory [25] and ductile Coulomb-Mohr theory [25] are not applied since the former is too conservative and the latter is suitable for unequal yield strengths. The distortion-energy theory predicts that yielding occurs when the distortion strain energy per unit volume reaches or exceeds the distortion strain energy per unit volume for yield in simple tension or compression of the same material. Mathematically, this theory is described using the von Mises stress, σ' which is defined as

$$\sigma' = \sqrt{\sigma_A^2 - \sigma_A \sigma_B + \sigma_B^2} \tag{3}$$

where σ_A, and σ_B are principal stresses. Based on this theory, yielding occurs when von Mises stress is larger than yielding strength (S_y).

B. Brittle Material

For brittle behavior, we choose modified Mohr over brittle Coulomb-Mohr [25] theory, since it is less conservative. The modified Mohr theory states that failure occurs whenever one of the principal stresses equals or exceeds the ultimate strength which can be written as

$$\sigma_A \geq S_u \text{ or } \sigma_B \leq -S_u \tag{4}$$

where S_u is the ultimate strength.

C. Task Requirements

To be able to apply normal and shear stresses by a normal-size conventional robot hand, the stresses applied by the hand are leveraged to result in the highest impact on the part. The bending stress for a circular beam subjected to a bending moment, M_b, can be obtained as,

$$\sigma_n = \frac{M_b c}{I} \tag{5}$$

where I is the second *moment of area*, and c is the radius of outer beam surface.

The shear stress resulted by twisting moment, M_t, acting on the same beam is given by

$$\sigma_t = \frac{M_t c}{P} \tag{6}$$

where P is the polar second moment of area.

In object failure, task wrenches are generated by the reaction of the object undergoing stress. The failing or yielding wrench vector, expressed as $w_y = [0,0,0,M_b,0,M_t]^T$, needs to be large enough such that it results in normal stress (5) and shear stress (6), satisfying the distortion-energy theory and modified Mohr theory for ductile, and brittle materials, respectively. Figure 4 shows two different, yielding wrench vectors on a Tomato plant. In this figure, two points of interest for failure at various locations are shown. Virtual circular beams are illustrated in Fig. 4. The virtual beams are considered to have circular profile covering the stem with any general shape. Yeilding wrench vectors ensure yielding/failing of the virtual beams, thus, yielding/failing of the stem. Mathematically,

Proposition 1: Wrench vector w_y fails or yields a ductile object if $\sigma' > S_y$.

Proposition 2: Wrench vector w_y fails or yields a brittle object if $\sigma_A \geq S_u$ or $\sigma_B \leq -S_u$.

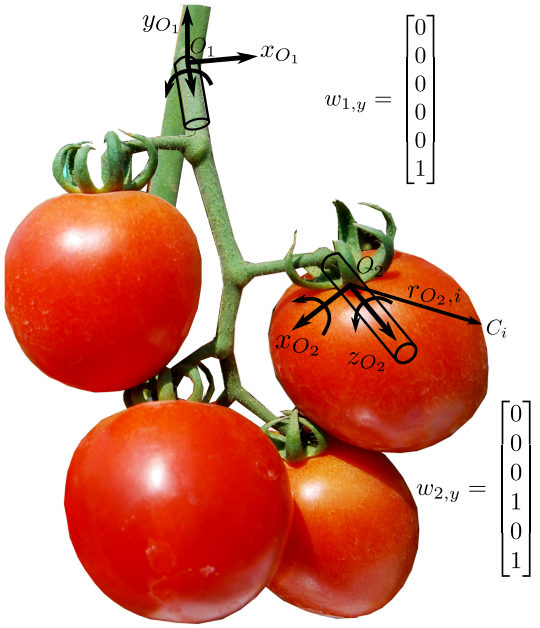

Fig. 4. Yielding wrench vectors and virtual circular beams on a Tomato plant. $r_{O_2,i}$ is the moment arm to the hypothetical contact point C_i.

Note that we can always change the grasp configuration and map any wrench to the point of interest; hence, planar principal stresses have only been considered without the loss of generality.

D. Task Optimization

In harvesting, there are cases of fruit clusters in which picking one fruit can damage surrounding ones. Hence, the grasp planner must consider restrictions on applying normal and shear stresses. An optimized w_y can be considered for the object in order to apply needed torque and moment to fail the object and at the same time avoid violating constraints on the amount of twist and deflection. Using Castigliano's theorem [25], *maximum deflection* results from moment M_b in (5) is given by,

$$\delta = \frac{M_b}{k_n} \tag{7}$$

where $k_n = \frac{2EI}{l^2}$ is the bending stiffness, l is the length of the beam, and E is the *Young's modulus* of elasticity. Similarly, the *maximum angle of twist* results from moment M_t in (6) is given by,

$$\theta = \frac{M_t}{k_t} \tag{8}$$

where $k_t = \frac{RP}{l}$ is the torsional stiffness, R is modulus of rigidity, and θ is measured in radian.

Defining Δ as the maximum allowable deflection and Θ as the maximum allowable twist (see Fig. 1), from (7) and (8) and using failure theories for ductile and brittle objects, the optimized wrench for failing the object is obtained as follows,

$$\begin{aligned} \underset{M_b,M_t}{\text{minimize:}} \quad & \|w(M_b,M_t)\| \\ \text{subject to:} \quad & \delta(M_b) \leq \Delta \\ & \theta(M_t) \leq \Theta \\ & \sigma' > S_y \text{ for ductile objects.} \\ & \sigma_A \geq S_u \text{ or } \sigma_B \leq -S_u \text{ for brittle objects.} \end{aligned} \tag{9}$$

According to our experiments, bending produces a larger portion of failing or yielding stress with less deflection since it is primarily leveraged with the length of the beam. One notable exception is when the volume of the fruit, e.g., Tomato, provides a long arm for applying torsion to the stem which results in relatively larger shear stress. Assuming the object shown in Fig. 3 is a fruit to be broken at the point O, one can easily show that the large moment arm vector, r_{oi}, provides high leverage for twisting. In such cases, the shear stress resulted from twisting will be comparable, if not larger than bending normal stress.

IV. Grasp Planning Method

A fully defined failure task can enable grasp planning. Given the locations of interest for the fracture, there are a small number of candidates for the grasp. The solution space can be furthered narrowed down by considering the capability of the gripper among the remaining candidates. The capability of the gripper is dictated by the saturation limits of the actuators and the contact friction.

A. Friction Identification

Contact points with friction are necessary for applying tangential force and avoiding slippage. It is assumed that a grasped object is rigid and the grasp consists of any number of hard contacts with friction. A rigid-body model is simple and appropriate for problems involving parts with low to moderate contact forces. In contrast, this type of modeling is not capable of describing large deformations due to large contact forces. To analyze the object deformations, one must introduce compliance into the contact model or use three-dimensional finite-element models [26]. Despite their accuracy, these models entail difficult numerical procedures and are computationally complex. The complexity of numerical models discourages the application of these types of models, particularly during grasp control. A hard contact model, on the other hand, can provide a computationally efficient trade off between identifying anisotropic friction behavior and the accuracy of the resulting model.

Contact forces, in the presence of friction, deviate from z-axis pointing in the direction of the inward surface normal (see Fig. 5(a)). Coulomb's law of friction is a common model for describing friction. If contact forces obey the Coulomb friction model, then they form the space of all admissible contact forces as a circular cone with opening angle $2tan^{-1}(\mu)$, where μ is the coefficient of friction. In other words, this model states the relation between the tangential component of a contact force, f_{ti}, and its normal component, f_{ni}, i.e., $\|f_{ti}\| = \mu \|f_{ni}\|$.

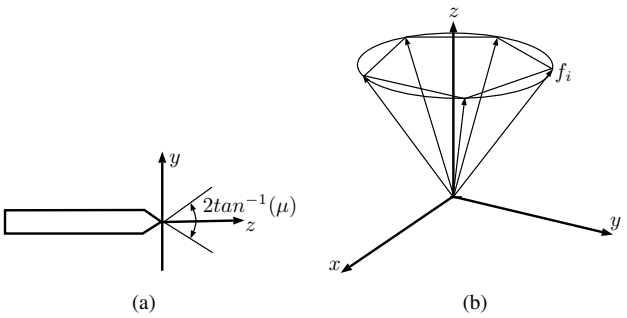

Fig. 5. For contact forces that obey the Coulomb friction model, they must be inside the friction cone. (a) Side view of a hard contact with friction, together with its coordinate system. (b) A friction cone which is approximated by a five-sided pyramid.

Coulomb friction model is not suitable for robotic harvesting due to high anisotropic behavior of crops. Therefore, We propose a new friction model that captures such anisotropies using experimental friction data as follows,

$$\|f_{ti}\| = u^T \begin{bmatrix} \mu_{xx} & \mu_{xy} \\ \mu_{xy} & \mu_{yy} \end{bmatrix} u \|f_{ni}\| \tag{10}$$

where u is the normalized 2D velocity direction, and μ_{xx}, μ_{yy}, and μ_{xy} are three friction coefficients along x and y directions as well as coupling between them. This model addresses the anisotropic frictional behavior of the object such as high latitudinal friction in a Wood beam surface due to the longitudinal orientation of its fiber cells [27]. This model is considered to be a cone whose base is not restricted to a circle and can vary in different directions (u). The proposed model is not computationally intensive and is obtainable during a pregrasp procedure.

Identification of μ_{xx}, μ_{yy}, and μ_{xy} in (10) require at least three different sets of data. Similar to the approach utilized by a human encountering a new object, we suggest a method in which the gripper is used to identify object's friction by touching the surface of the object. The gripper starts inserting a small amount of normal contact force, $\|f_{ni}\|$ while moving and measuring the reaction forces, $\|f_{ti}\|$. The contact force is considered to be small to avoid damage to the object. The process is repeated at least in three different directions on the object to identify all three friction coefficients.

B. Grasp Wrench Space

The ability of wrench exertion is highly dependant on friction. Assuming that the value of the wrench that needs

to be applied to the object is known, one must express this wrench in terms of the friction forces and associated normal contact forces. To this end, the nonlinear friction cone is often approximated with an n_s-sided pyramid (see Fig 5(b)). A given contact force is then decomposed as a positive linear combination of the force vectors spanning the n_s-sided friction pyramid, i.e.,

$$f_{c_i} = \sum_{i=1}^{n_s} \alpha_i f_i, \quad \text{for} \quad \alpha_i \geq 0 \tag{11}$$

where each f_i vector has unit z-component, and $\sum_{i=1}^{n} \alpha_i$ corresponds to the normal component of the contact force. Each force vector f_i results in an object wrench that makes up the Grasp matrix. The Grasp matrix can be seen as the column space of wrenches contributed by all contacts. One of the most important properties of a grasp is its capability of inserting desired contact forces in a given grasp configuration.

In grasp analysis, knowing the space of wrenches that can be applied to the object is always a notion of interest. The grasp wrench space (GWS) is defined as the space of wrenches that satisfy (1). This space is equal to the convex hull of the Grasp matrix, which can be efficiently computed using the Quickhull algorithm [28]. The GWS is highly dependent on friction coefficient. The GWS for a force-closed grasp contains a neighborhood of the origin. To calculate the GWS, the friction cone approximated with an n_s-sided pyramid is used. A pyramid with more sides gives a more accurate triangulation and results in a better visual representation and higher accuracy of the GWS. However, for grasp evaluation purposes the approximation is made with less number of sides which can dramatically change the computational intensity of the evaluation method.

C. Grasp Evaluation Metric

In this section, a grasp evaluation index is introduced based on the grasp wrench space (grasp capability). This index accounts for the specific actuation of the robotic hand using a transmission matrix. A transmission matrix, T, is defined to relate actuators torque vector to joints torque vector as follows,

$$t = T^T \tau \tag{12}$$

where $\tau \in R^{n_q}$ is the torque vector for a robotic hand with n_q joints, and $t \in R^{n_a}$ is the torque vector of n_a actuators. The definition represents generic actuation of the hand and can be modified to represent a specific actuation form. In other words, the transmission matrix is a unit matrix in a fully actuated hand whereas, in an under-actuated hand, the matrix can be modified accordingly. The mapping from contact forces to the robot joint torques for a grasp with n_c contact points can be expressed as,

$$\tau = \tilde{J}^T f \tag{13}$$

where $\tilde{J} \in R^{3n_c \times n_q}$ is the Jacobian matrix of a fully-actuated hand. The definition of the Jacobian matrix is usually expanded for under-actuated mechanisms to include the transmission matrix, $J = \tilde{J}T$ [29]. A defective class of grasping occurs when certain contact forces produce no actuation torques or vice versa. In other words, there are certain contact force vectors inside the left null space of the Jacobian matrix ($\mathcal{N}(J^T)$) which cannot be generated by joint actions.

Any robotic hand with hard contact and friction can transfer three force components to an object. Our proposed friction model determines the tangential force components in any direction according to the normal force. Knowing the saturation limits for the actuation and having a friction model, one can obtain the maximum wrench that the robot hand can exert on an object. Taking both the gripper grasp capability and task-oriented information into account, the following grasp evaluation metric is proposed,

$$Q = \min_i \frac{\|w_i^*\|}{\|w_{i,y}\|}, \quad \text{for} \quad i = 1, ..., n_t \tag{14}$$

where w_i^* is the maximum applicable wrench in i direction, $w_{i,y}$ is the i^{th} failing or yielding task vector obtained in (9), and n_t is the number of failing or yielding task vectors. This grasp quality index requires repeated identification of the maximum wrench that can be applied by the gripper to the object in the direction defined by a task vector.

In order to maximize an applicable wrench along a given direction, the problem is formulated as a linear optimization problem in which $\|w_i\|$ is the value that we wish to maximize subject to (12), (13). The optimization problem can be expressed as follows,

$$\begin{aligned} \underset{i}{\text{maximize:}} \quad & \|w_i\| \\ \text{subject to:} \quad & d_i \|w_i\| - Gf = 0 \\ & f \in \mathcal{N}(G) \\ & f \notin \mathcal{N}(J^T) \end{aligned} \tag{15}$$

where d_i is defined as $d_i \triangleq \frac{w_{i,y}}{\|w_{i,y}\|}$ and all other variables are as defined previously. The first constraint ensures that the applied wrench Gf remains within the failing or yielding task vector direction. The second constraint ensures that contact forces maintain within the friction cone and result in internal forces. The third constraint ensures the controllability of the internal forces to produce the desirable object wrench.

V. Results

To validate the proposed grasp quality metric and the friction identification method, failing of both brittle and ductile objects were considered. Considering ductile materials is important since it represents a large group of biological substrates that behave in this manner. Yielding such materials eventually, leads to breaking them into pieces in a brittle manner. In other words, yielding a ductile stem helps *failing* it afterward. A circular beam made of Steel was considered as an extreme example of a ductile material.

We also considered a Wood square beam to demonstrate the validity of the approach used for generalizing all beam profiles. The Wood beam was chosen to mimic the behavior of a tough stem and some of its important biological behaviors such as Greenstick fracture and buckling. The complete failing process considering the probable Greenstick fracture was implemented to show the grasping capability of the results.

Lastly, failing a Tomato stem was conducted to show the validity of the grasp evaluation method in handling the variations of the failure task from the one used to obtain the optimum wrench. As shown in Fig 4, the whole cluster can be harvested (using the wrench vector $w_{1,y}$), or a Tomato can be harvested from its cluster (using the wrench vector $w_{2,y}$) [30]. Harvesting a Tomato from its cluster is considered in our experiment to demonstrate the ability of our algorithm to avoid any motions that result in damaging the surrounding Tomatoes in the cluster.

A. Experimental Setup

In a room with controlled humidity and temperature, mechanical properties for Steel, Wood, and Tomato were considered. Table 1 summarizes the properties of these objects in 40% relative humidity and 21°C. In [31], methods for measuring bending and torsional stiffness were suggested, eliminating the need for knowing the object properties in advance. In this paper, we assume that the material properties and the location of fracture are given to the grasp planner for the sake of simplicity. The target object was fixed from one end to the table and the other end kept loose in the air. At each experiment, the gripper grasped the object above the fixed point. The object was grasped with an under-actuated hand with two fingers. A robotic arm was used to control the gripper's orientation in order to follow a planar motion around the fixed point. The robot arm was moved slowly to not violate the quasistatic conditions.

Steel round beam radius (m)	0.003
Steel Young's modulus (N/m^2)	207×10^9
Steel yield strength (N/m^2)	220×10^6
Wood squire beam dimensions ($m \times m$)	0.007×0.007
Wood Young's modulus (N/m^2)	8.9×10^9
Wood ultimate strength (N/m^2)	40×10^6
Tomato outer radius (m)	0.035
Tomato stem radius (m)	0.0015
Tomato Young's modulus (N/m^2)	7.0×10^8
Tomato ultimate strength (N/m^2)	30×10^6

Tab. 1. Properties of materials [25], [32], [22]

We used a Kuka Light-Weight Robot (LWR) IV and a CRS Robotics under-actuated gripper for conducting our experiments. Two load cells in each finger and an ATI 6-axis force/torque sensor at the wrist were used for acquiring data (see Fig. 6(a)). We intentionally selected a simple gripper and a finger structure to facilitate our study and the evaluations therein without compromising the intended grasp scenario required for the study. The design of more enhanced fingers is reported in [29]. The utilized finger structure is separately shown in Fig. 6(b). This figure shows the finger tip that was in contact with the object. The contact region was a plate screwed to the load cell. The load cell was also screwed to the finger fixture which was actuated by the gripper. The configuration allowed to measure contact forces using the load cell.

To exploit the capabilities of Kuka LWR controller along with peripheral tools and sensors, we developed an open-source KUKA UI (https://github.com/mahyaret/KUKA-UI). This is a comprehensive computer interface that allows for seamless integration and synchronous control of additional peripheral tools and third-party sensors with Kuka Controller. The program was developed based on Kuka Fast Research Interface (FRI) to enable real-time control of the robot. Type II Reflexxes Motion Library was used to generate an online trajectory for Kuka LWR in different control modes.

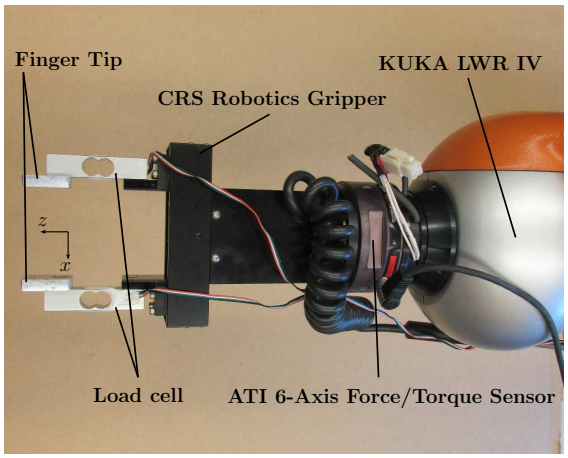

(a)

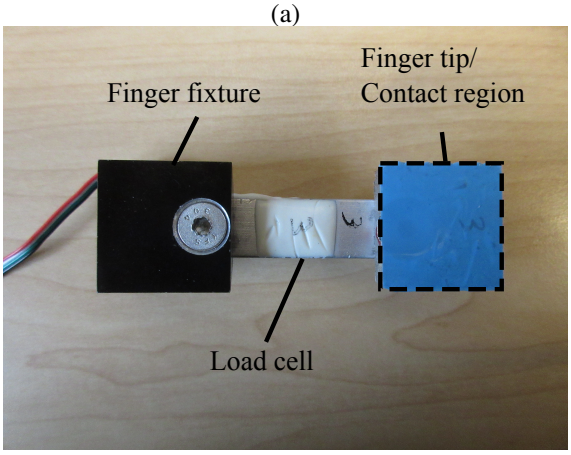

(b)

Fig. 6. Experimental hardware setup. (a) Gripper and the force/torque sensor attached to the manipulator. (b) Finger structure consisting of finger tip plate, load cell, and the fixture. The contact region is the area on the finger tip which is in contact with the object.

CRS Robotics gripper is a planar under-actuated open/close gripper. The gripper has two fingers that are actuated simultaneously with a single DC motor. In this 2D experimental setting, the force-closure grasp was achieved assuming hard contact with friction. The Jacobian and transmission matrices for this gripper are given by,

$$J = \begin{bmatrix} 0 & 0 & 0 & -1 & 0 & 0 \\ 1 & 0 & 0 & 0 & 0 & 0 \end{bmatrix}^T, T = \begin{bmatrix} 1 \\ -1 \end{bmatrix}$$

The Grasp matrix for this two contact point planar scenario is given by,

$$G = \begin{bmatrix} 1 & 0 & 0 & 1 & 0 & 0 \\ 0 & 0 & 0 & 0 & 0 & 0 \\ 0 & 0 & 0 & 0 & 0 & 0 \end{bmatrix}$$

Internal forces which were in the null space of the Grasp matrix, excluding those within the left null space of Jacobian

matrix were obtained. These internal forces allowed to squeeze the object without resulting in any object motion. The calculated internal forces are as follows,

$$A = [-0.7071, 0, 0, 0.7071, 0, 0]^T$$

Without losing generality, the Grasp matrix for all grasp scenarios was considered to be identical by assigning the origin of the reference frame at the yielding point of the object.

We used the gripper itself as our frictional test device. The robot fingers applied small magnitude normal forces to the surface of the object while moving along the object surface in different tangential directions (see Fig. 7). The normal forces were regulated using the load cells embedded in the fingers. The tangential forces of the friction force were measured using the ATI 6-axis force/torque sensor. In practice, normal forces produce chattering effects during contact with hard surfaces due to unavoidable measurement noises. A PID controller enhanced with Kalman filter was used to regulate normal forces.

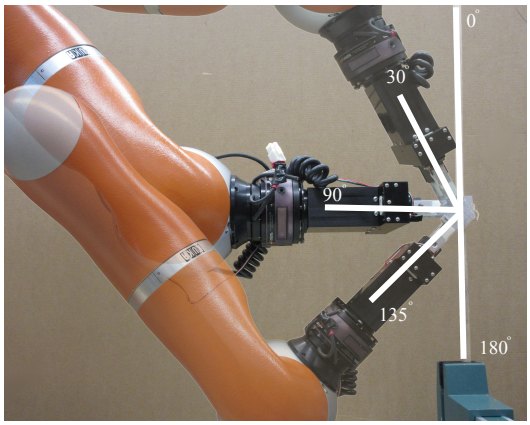

Fig. 7. Tangential directions that the robot fingers apply low magnitude normal forces to the surface of the object while attempting to move upward. Tangential direction of 30°, 90°, and 135°.

B. Experimental Results

1) Friction Identification: Different normal contact forces were regulated, and the tangential reaction forces were measured. Figure 8(a), (b), and (c) depicts measured friction forces of Steel, Wood, and Tomato skin when different normal forces were applied by the fingers on the object while moving upward along the surface of the object. The figures include the results of grasping the object at different orientations, e.g., Figure 8(a) shows the results for 30°, 90°, and 135° orientations for Steel, Figure 8(b) for 30°, 60°, and 135° orientations for Wood, and Figure 8(c) for 30°, 90°, and 120° orientations for Tomato skin. These figures provide a comparison of the frictional behavior of the objects and validate our earlier assumption regarding the anisotropy of friction forces. In particular, friction forces in Tomato skin experiment significantly changes for different orientations. Steel and Wood, on the other hand show homogeneous behavior as expected. These experiments substantiated the importance of frictional tests. In fact, without frictional data, the friction coefficient estimation is far from accurate.

The normal and tangential forces were used to obtain friction coefficients. Different friction coefficients for the examined materials are provided in Tab. 2. One can note that μ_{xy} can be negative while the matrix $[\mu_{xx}, \mu_{xy}; \mu_{xy}, \mu_{yy}]$ remains positive definite. The highest friction direction provides important information for choosing the orientation of the grasp. To validate the identified friction model additional experiments using different normal forces from those used for model identification were conducted. Normal forces in new orientations were applied and the corresponding reaction forces were measured. The results were then compared with those predicted by the identified model. The results of these experiments are summarized in Fig. 8(d), (e), and (f). As seen, the applied contact (normal) forces used in the experiments were two times larger than those used for identification and the orientation of the gripper was chosen to be different than those used for initial measurements. The data shows relatively good match, validating the accuracy of the friction model and its capability of handling the anisotropic behavior of the object.

Material	μ_{xx}	μ_{xy}	μ_{yy}
Steel	0.2031	-0.0073	0.2106
Wood	0.2255	-0.0436	0.2639
Tomato	0.1749	0.0272	0.3322

Tab. 2. Friction constants

The Anisotropic behavior of the object results in having different friction coefficients in different directions. As such, the friction cones for such objects do not follow the typical circular form of the friction cone for isotropic materials (see Fig. 5(b) as an example). Figs 8(g), (h), and (i) show the variations of the friction cone from a circular shape corresponding to the values of the friction constants. The shapes of these cones depend on other parameters and can vary with changes in the humidity and temperature of biological beams. These observations clearly show the importance and necessity of our proposed friction identification method that is capable of capturing the variations of the friction in particular for biological objects.

The proposed identification method can serve as an initial object assessment for obtaining friction parameters that can then be used for grasp planning. The process is intended to be fast and avoid damage to the object surface.

2) Gripper Capability: To demonstrate the capabilities of the gripper, the grasp wrench space, the GWS was calculated using all admissible forces that were inside the friction cone (see Fig. 8(j), (k), and (l)). We used the friction cones for the three selected materials in our study (i.e., Steel, Wood, and Tomato skin) to obtain the GWS in each case. The friction cones were approximated to have 15 sides each. A two-contact point grasp configuration was considered so as to reflect the structure of the CRS robotic gripper. Figure 8(j), (k), and (l) show the grasping capability of the gripper for the applied normalized wrench.

The anisotropy of the friction forces is clearly reflected in the asymmetrical shape of the two-contact point the GWS. Also, as seen, the GWSs for all three materials contain a neighborhood of the origin, showing the force-closure properties of

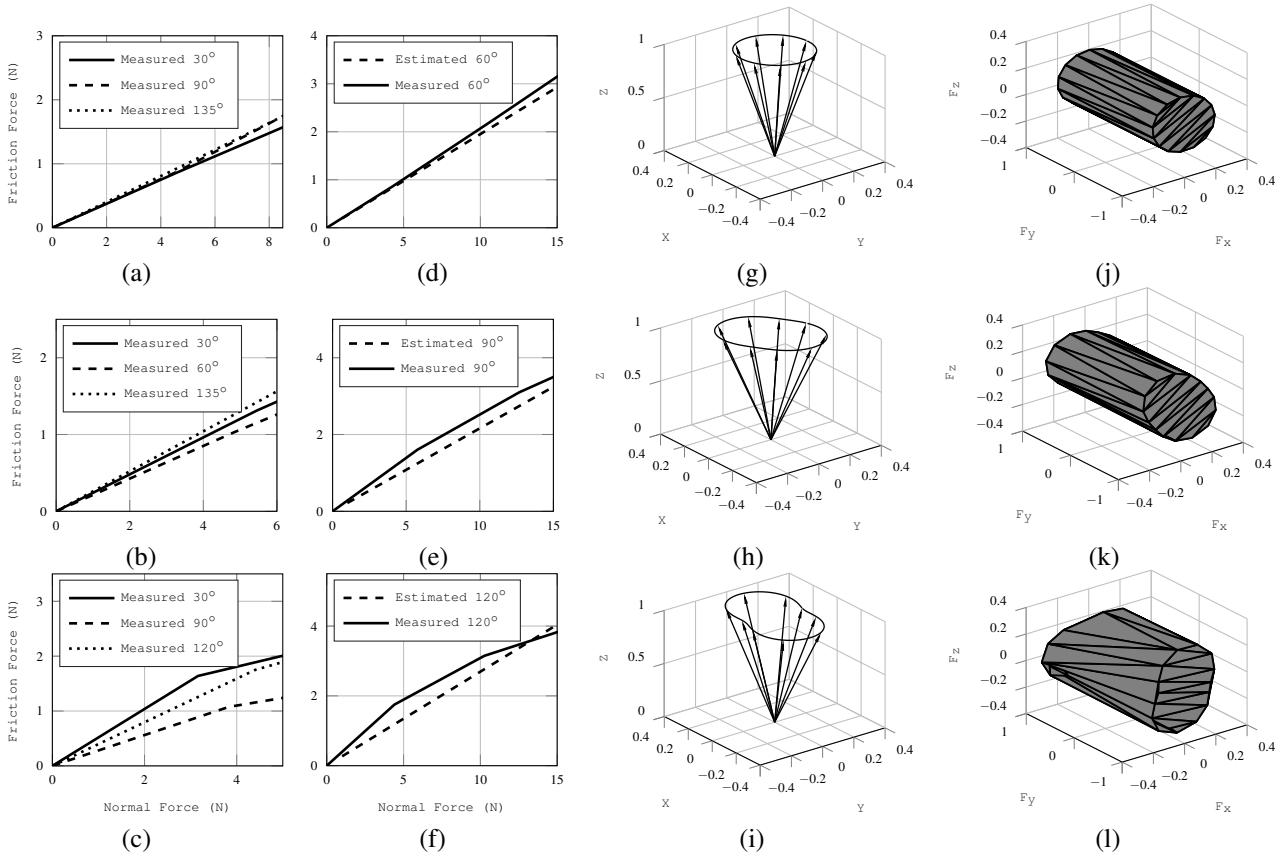

Fig. 8. (a) Anisotropic behavior of the friction in a Steel beam. (b) Anisotropic behavior of the friction in a Wood beam. (c) Anisotropic behavior of the friction in Tomato. (d) Steel beam friction model validation at 60°. (e) Wood beam friction model validation at 90°. (f) Tomato surface friction model validation at 120°. (g) Steel beam friction cone. (h) Wood beam friction cone. (i) Tomato surface friction cone. (j) Steel beam normalized grasp wrench space using 15-sided pyramid friction. (k) Wood beam normalized grasp wrench space using 15-sided pyramid friction. (l) Tomato normalized grasp wrench space using 15-sided pyramid friction.

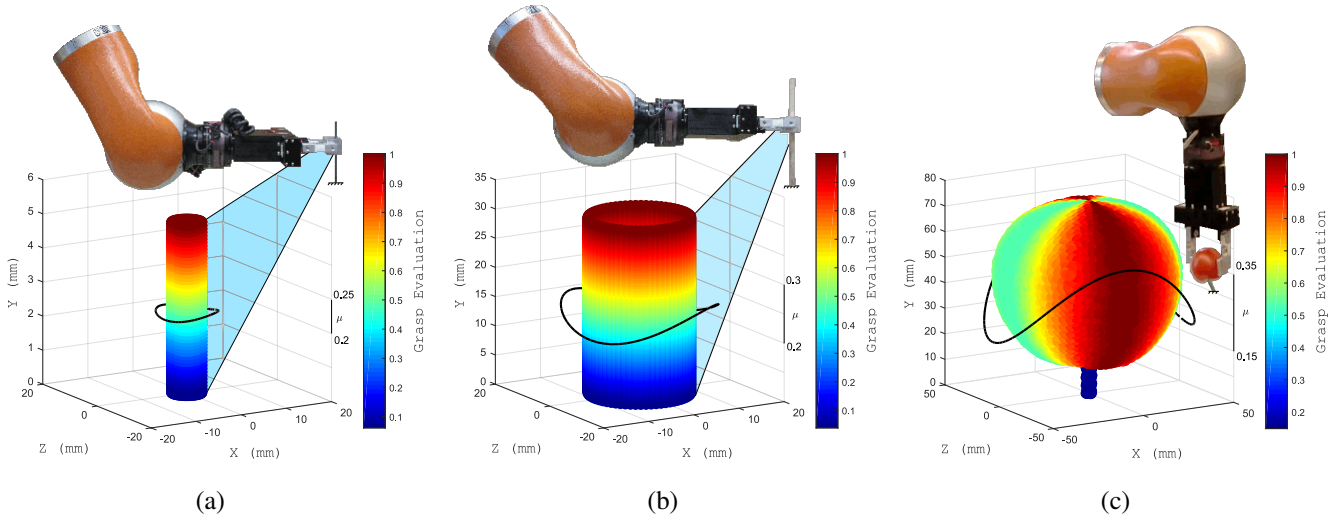

Fig. 9. Grasp planner results for Steel beam, Wood beam, and Tomato. The intended yielding location is color-coded by the value of grasp evaluation metric. Grasp evaluation values and their friction-dependent variations for (a) Steel, (b) Wood, and (c) Tomato. The grasp evaluation metric suggests the optimal orientation for applying torsion.

the grasp which allows withstanding any external forces using an appropriate contact force. For instance, if the contact forces applied to the Steel beam are regulated to be $10N$, the grasp configuration can then tolerate up to $2N$ of an external force in z-direction (see Fig. 8(j)).

The results shown in these figures are rather intuitive but they highlight the importance of considering these results during grasp planning and control. The results show that a grasp with higher friction can counterbalance greater external forces. Moreover, if an object is held in areas with higher friction, these areas can provide more stable grasp against external disturbances.

3) Grasp Planner: The grasp planner proposed earlier in (14) can quantify suitable grasps. The inputs of the grasp planner are the GWS, task information, and the fracture location, and its output are the distinguished areas optimum for applying failure stress. The GWS expresses gripper capabilities using measured friction forces and task information in our case was obtained using (9). The fracture location was randomly selected on the object. The grasp planner ensures that by obtaining the calculated grasp configuration, the manipulation process can be conducted without any slippage or unexpected object damage.

Using (9) for the Steel beam, $\Delta \approx 60^\circ$ and $\Theta \approx 60^\circ$, we obtained the wrench vector of $w_y = [0,0,0,132,0,0]$. The grasp planner output for the Steel beam is shown in Figure 9(a). The grasp planner value is normalized and color-coded in this figure. The areas with red color correspond to the highest evaluation index. These areas are intuitively suitable for bending since they provide the largest leverage on yielding stress. The friction variations are also included in Fig. 9(a). There is a negligible change in grasp planner output with respect to the direction of the applied force. This is due to the fact that bending moment has a much larger effect on yielding the beam without much reliance on friction than the shear stress. The target point for yielding the beam was selected randomly. We considered a maximum arm for the bending moment of $5mm$. This limitation forces the grasp planner to use only $5mm$ leverage for applying bending moment. This small length was considered intentionally to address the tight space requirement imposed by the conditions of the farming environment.

Using (9) for the Wood beam, $\Delta \approx 60^\circ$ and $\Theta \approx 60^\circ$, we obtained the wrench vector of $w_y = [0,0,0,138,0,0]$. The grasp planner output for the Wood beam is shown in Fig. 9(b). A similar process as the one applied to the Steel beam was repeated for a virtual cylindrical beam that approximate the square profile of the Wood beam. Fig. 9(b) shows the results of the grasp planner similar to those obtained for the Steel beam. As seen, there is a negligible change in grasp planner output with respect to the direction of the applied force since bending moment in the Wood beam is also a major contributing factor to yielding the object. A maximum $30mm$ arm for bending moment was considered since the Wood beam was much thicker than Steel beam (130%) requiring much higher bending moment to yield. This arm is still small enough to be applicable to harvesting scenarios. The similarities of the results for the Wood and Steel beams are due to the heavier reliance of both cases on the bending moment.

Using (9) for the Tomato, $\Delta \approx 20^\circ$ and $\Theta \approx 40^\circ$, we obtained the wrench vector of $w_y = [0.0,0.0,0.0,0.0,0.0,0.2]$. The grasp planner output for the Tomato is shown in Fig. 9(c). The results are shown in similar color-coded format. In this case, motion limitations are considered in the task definitions as illustrated in Fig. 1. As it can be seen in this figure, the robot cannot bend and twist the Tomato indefinitely since it will damage the surrounding Tomatoes. Using (9), we obtained the wrench vector similar to $w_{2,y}$ in Fig. 4 except with near zero bending moment around x_{O_2} axis. The most effective grasp areas in Fig. 9(c) are those shown in red. This figure indicates that applying torsion is the most effective way of harvesting. The result is intuitive given that fact that the comparatively large fruit size provides a larger arm for applying torsional moment and dominating the effect of shear stress. In other words, in this case, the shape of the fruit itself dictates the leverage required for failing the stem. Fig. 9(c) clearly shows that the stem itself has a much lower value of grasp index (blue color) in comparison to the body of the Tomato that provides a much better leverage for twisting (red color). Also, as expected, the areas with lower friction require larger normal forces that those with higher friction. However, larger normal forces can result in unwanted damage when dealing with a perishable material such as fruit and vegetables. For Tomato, we fed the approximate fruit size to the planner, in addition to the target beam dimensions which was the stem of the fruit. As seen, the proposed planner does not require high accuracy object model; instead, it uses approximate boundary representation of the object. In agricultural robotics, the main topological items are known for the potentially ripped crops.

Based on the task information, the grasp planner showed different levels of dependencies on the friction. Twisting an object required higher normal forces and frictions in comparison with the bending of the object. The reason for this result lies in the fact that in our system the gripper's pose can be configured such that the bending wrench vector remains inside the Grasp matrix null space. As mentioned earlier, the null space of Grasp matrix is the subspace of internal forces that result in wrench intensity with no object motions. Hence, by avoiding in-hand object motions, the grasp planner can achieve a desired outcome without relying heavily on the friction forces.

4) Failure Validation: Based on the results from the grasp planner suitable areas for grasping as well as the strategy for failing the object were determined. These grasp sets were validated by applying the failure stress on the object and investigating whether the grasp was capable of withstanding the stress and maintaining its configuration. In these experiments, the gripper (i.e., CRS Robtics) grasped the object at points defined by the grasp planner. The gripper and the object were considered as a single load attached to the end-effector of the robot arm (Kuka LWR IV). The robot moved in the direction suggested by the planner until failure occurred. All contact forces were continually adjusted according to the external wrenches during this process.

For Wood and Steel beams, the grasp planner results suggested bending rather than twisting as an effective method and it also specified that bending should be done from the longest distance possible from the target point. A maximum

distance of 5*mm* for Steel beam and 30*mm* for the Wood beam was considered. The determined wrenches were applied at these distances until the Wood beam snapped and Steel beam yielded. Figure 10 depicts the measured reaction contact forces while failing these objects. Comparing this figure with Fig. 2, shows that by continuously orienting the gripper (as a function of time) around the predetermined yielding location, larger reaction contact forces, as shown in Fig. 10(a), were measured. The experiment was continued until the distortion became permanent and the resisting moment dropped. The normal stress in this process for the Steel beam is $2.4770 \times 10^8 N/m^2$ which is larger than its yielding strength. As for the Wood beam, snapping occurred after the Greenstick fracture was observed as shown in Fig. 10(b). As seen in this figure, the contact forces slightly drop shortly before the final drop of the grasp contact forces. The normal stress for the Wood beam was calculated as $4.3163 \times 10^7 N/m^2$ which is more than its ultimate strength.

For the case of detaching the Tomato fruit from its stem, the grasp planner results suggested to apply torsion rather than bending. There are several directions in 3D space for applying torsion on the Tomato. Since, the friction in Tomato skin was shown to be anisotropic, applying contact forces in certain directions could raise the possibility of slippage. As such, the grasp planner used the friction model data to calculate the best orientation for applying torsion. Based on these observations, the robot was commanded to twist the Tomato around its stem. No slippage was observed, and the grasped object, i.e., Tomato remained locked in the gripper. The shear stress for Tomato torsion was measured at $3.4368 \times 10^7 N/m^2$.

VI. Discussion

This paper provided a framework for obtaining grasp planning for harvesting. This framework was not limited to harvesting a particular crop; it offered an algorithm first to define the proper task then plan for the grasp. As it was shown in Fig. 4, different tasks can be defined to fail the plant from any point of interest.

The stem of crops can behave in brittle or ductile manner. To break a ductile stem, it needs to be yielded first. Yielding ductile materials causes cracks in their structure which then leads to breaking them into pieces in a brittle manner. Steel was considered as an extreme example of a ductile material. The proposed algorithm assumed that the beam has a circular profile; however, no plant has a perfect circular profile. For addressing this issue, a virtual circular beam was considered to cover the original stem. For this reason, a square Wood beam was considered as an extreme example of similar cases. Lastly, failing a Tomato stem was conducted to show an example of how to use the proposed approach for an actual harvesting scenario. Farmers may prefer harvesting a cluster of tomato rather than just harvesting one tomato from its stem. Formulating such problem is also easily possible by using different, yielding wrench vector (see Fig. 4).

It is worth noting that the grasp planner considers contact forces magnitude to comply with friction force requirements and damage avoidance. For instance, it is possible to apply higher contact forces and torsion in directions *not* recommended by grasp planner. In that case, we would probably be successful in failing the object; however, the object could be damaged due to excessive contact forces.

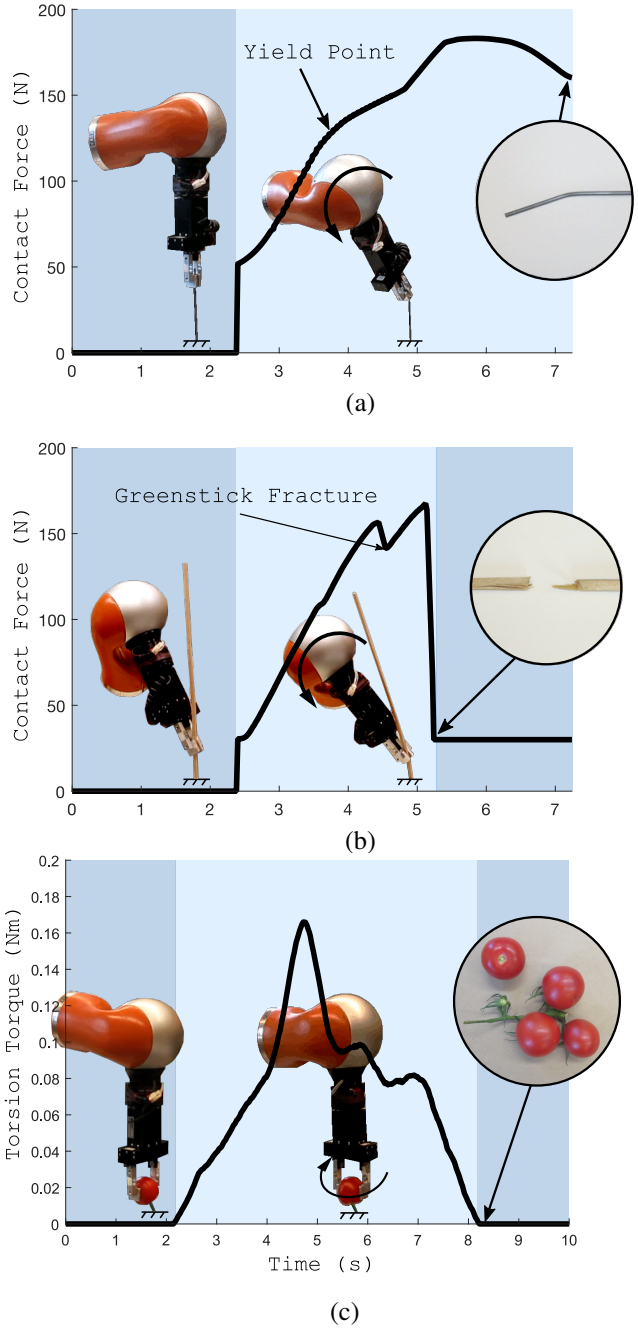

Fig. 10. Failure test results. (a) Yielding Steel beam by means of permanently distorting it. (b) Failing Wood beam by means of breaking it to pieces. The Greenstick fracture behavior can be explained by anisotropy between the radial and tangential directions. (c) Failing Tomato by means of harvesting it from its stem.

Friction is an essential part of any grasp planning method and it is often assumed as an a priori information require to solve the grasp problem. The friction model and identification method presented in this work provided a practical solution to measure the actual value of the friction. The proposed friction identification method can be used in any task-oriented

grasp planing as a preplanning procedure. This procedure was not required to be repeated during the grasp operation unless due to the variations of environmental parameters that can affect the friction property. The friction property can show an anisotropic behavior which is well studied theoretically in the literature. In this work, a new method inspired by the human pre-manipulation process to measure the friction was introduced. The method was fast and considered anisotropy in friction. Using this method, the true nature of the friction force along different surface directions was captured. This model was particularly important for planning a breaking task while avoiding slippage by accounting maximum friction force along different directions against large tangential reaction force inherent in breaking task.

VII. Conclusions

This paper considered the problem of purposefully failing/yielding an object. A grasp planner designed for this purpose was introduced. A planner which combined the capabilities of the gripper and the mechanical properties of the target object was introduced to provide the best grasp candidates for the object failure. It was shown via mechanical failure theories and experimental results that bending produced more effective failure stress when the twisting arm was comparatively short, or friction was not enough. On the other hand, it was shown that when a large twisting arm was available, torsion could be more effective especially when there were space restrictions for bending the object. For instance, in robotic harvesting, where fruits provide a long twisting arm around the stem, torsion can be more efficient compared to bending to avoid damaging other surrounding fruits. While these results are intuitive and match our heuristic approach in harvesting, they highlight and validate the effectiveness of the proposed grasp planner in obtaining optimum solution based on current measured data.

Given the important role that friction plays in failure grasp, an enhanced friction model was proposed. In the proposed method, we examined the target object before grasping for measuring the friction between the gripper and the object. The friction modeling and measurement experiments allowed us to predict the capability of the gripper for torsion torque insertion required in twisting an object. Our proposed model is able to capture more complex frictional behavior such as anisotropy which is the case for most agricultural products. Since temperature and humidity can also affect friction, the proposed friction identification method is proved to be an important means of obtaining appropriate data for more accurate grasp planning. The proposed approach uses gripper in a similar way humans use their hands to elicit mechanical properties of new materials.

APPENDIX

Nomenclature

Grasp Analysis

n_a	Number of actuated joints of hand
n_c	Number of contacts
n_q	Number of joints of hand
n_s	Number of sides for friction pyramid approximation
$G \in R^{6\times 3n_c}$	Grasp matrix
$J \in R^{3n_c\times n_a}$	Jacobian matrix
$T \in R^{n_q\times n_a}$	Transmission matrix
$c_i \in R^3$	The position of contact point i
$O \in R^3$	Object origin (desired failure position)
μ	Coefficient of friction
g	Dimension of homogeneous solution space for the quasistatic manipulation model
$\tau \in R^{n_q}$	Torque vector
$f \in R^{3n_c}$	Contact forces vector
$f_i \in R^3$	Friction pyramid vertex i
$w_{i,max} \in R^6$	Maximal applicable wrench

Load and Stress Analysis

σ'	von Mises stress
Δ	Maximum allowable object deflection
Θ	Maximum allowable angle of object twist
E	Young's modulus
k_n	Bending stiffness
k_t	Torsional stiffness
M_b	Bending moment
M_t	Twisting moment
n_t	Number of failing/yielding task vectors
R	Modulus of rigidity
S_u	Object ultimate strength
S_y	Object yielding strength
$w_y \in R^6$	Failing/yielding wrench vector

References

[1] A. Van Casteren, W. Sellers, S. Thorpe, S. Coward, R. Crompton, and A. Ennos, "Why don't branches snap? the mechanics of bending failure in three temperate angiosperm trees," *Trees*, vol. 26, no. 3, pp. 789–797, 2012.

[2] A. Bicchi and V. Kumar, "Robotic grasping and contact: A review," in *Robotics and Automation, 2000. Proceedings. ICRA'00. IEEE International Conference on*, vol. 1. IEEE, 2000, pp. 348–353.

[3] A. Sahbani, S. El-Khoury, and P. Bidaud, "An overview of 3d object grasp synthesis algorithms," *Robotics and Autonomous Systems*, vol. 60, no. 3, pp. 326–336, 2012.

[4] J. Bohg, A. Morales, T. Asfour, and D. Kragic, "Data-driven grasp synthesisa survey," *IEEE Transactions on Robotics*, vol. 30, no. 2, pp. 289–309, 2014.

[5] M. Abdeetedal and M. R. Kermani, "Optimal grasp synthesis to apply normal and shear stresses of failure in beams," in *Advanced Intelligent Mechatronics (AIM), 2016 IEEE International Conference on*. IEEE, 2016, pp. 395–400.

[6] ——, "Grasp evaluation method for applying static loads leading to beam failure," in *Intelligent Robots and Systems (IROS), 2017 IEEE/RSJ International Conference on*. IEEE, 2017, pp. 5999–6004.

[7] F. Veiga, H. van Hoof, J. Peters, and T. Hermans, "Stabilizing novel objects by learning to predict tactile slip," in *Intelligent Robots and Systems (IROS), 2015 IEEE/RSJ International Conference on*, Sept 2015, pp. 5065–5072.

[8] X. A. Wu, N. Burkhard, B. Heyneman, R. Valen, and M. Cutkosky, "Contact event detection for robotic oil drilling," in *Robotics and Automation (ICRA), 2014 IEEE International Conference on*, May 2014, pp. 2255–2261.

[9] G. D. Maria, P. Falco, C. Natale, and S. Pirozzi, "Integrated force/tactile sensing: The enabling technology for slipping detection and avoidance," in *Robotics and Automation (ICRA), 2015 IEEE International Conference on*, May 2015, pp. 3883–3889.

[10] N. Sommer and A. Billard, "Multi-contact haptic exploration and grasping with tactile sensors," *Robotics and Autonomous Systems*, vol. 85, pp. 48–61, 2016.

[11] S. El-Khoury, R. De Souza, and A. Billard, "On computing task-oriented grasps," *Robotics and Autonomous Systems*, vol. 66, pp. 145–158, 2015.

[12] C. Borst, M. Fischer, and G. Hirzinger, "Grasp planning: How to choose a suitable task wrench space," in *Robotics and Automation, 2004. Proceedings. ICRA'04. 2004 IEEE International Conference on*, vol. 1. IEEE, 2004, pp. 319–325.

[13] Z. Li and S. S. Sastry, "Task-oriented optimal grasping by multifingered robot hands," *IEEE Journal on Robotics and Automation*, vol. 4, no. 1, pp. 32–44, 1988.

[14] X. Zhu and J. Wang, "Synthesis of force-closure grasps on 3-d objects based on the q distance," *IEEE Transactions on robotics and Automation*, vol. 19, no. 4, pp. 669–679, 2003.

[15] L. Han, J. C. Trinkle, and Z. X. Li, "Grasp analysis as linear matrix inequality problems," *IEEE Transactions on Robotics and Automation*, vol. 16, no. 6, pp. 663–674, 2000.

[16] T. Callier, H. P. Saal, E. C. Davis-Berg, and S. J. Bensmaia, "Kinematics of unconstrained tactile texture exploration," *Journal of neurophysiology*, vol. 113, no. 7, pp. 3013–3020, 2015.

[17] T. Yoshioka, J. C. Craig, G. C. Beck, and S. S. Hsiao, "Perceptual constancy of texture roughness in the tactile system," *The Journal of Neuroscience*, vol. 31, no. 48, pp. 17 603–17 611, 2011.

[18] M. Janko, R. Primerano, and Y. Visell, "On frictional forces between the finger and a textured surface during active touch," *IEEE transactions on haptics*, 2015.

[19] F. P. Beer, E. R. Johnston, and J. T. DeWolf, *Statics and mechanics of materials*. McGraw-Hill Education, 2017.

[20] E. Farnioli, M. Gabiccini, and A. Bicchi, "Quasi-static analysis of synergistically underactuated robotic hands in grasping and manipulation tasks," in *Human and Robot Hands*. Springer, 2016, pp. 211–233.

[21] M. C. Koval, N. S. Pollard, and S. S. Srinivasa, "Pre-and post-contact policy decomposition for planar contact manipulation under uncertainty," *The International Journal of Robotics Research*, vol. 35, no. 1-3, pp. 244–264, 2016.

[22] A. J. Matas, G. López-Casado, J. Cuartero, and A. Heredia, "Relative humidity and temperature modify the mechanical properties of isolated tomato fruit cuticles," *American journal of botany*, vol. 92, no. 3, pp. 462–468, 2005.

[23] J. Cáceres, A. Márquez, O. R. Oellermann, and M. L. Puertas, "Rebuilding convex sets in graphs," *Discrete Mathematics*, vol. 297, no. 1, pp. 26–37, 2005.

[24] A. Tekkaya, J. Allwood, P. Bariani, S. Bruschi, J. Cao, S. Gramlich, P. Groche, G. Hirt, T. Ishikawa, C. Löbbe *et al.*, "Metal forming beyond shaping: Predicting and setting product properties," *CIRP Annals-Manufacturing Technology*, vol. 64, no. 2, pp. 629–653, 2015.

[25] J. E. Shigley, *Shigley's mechanical engineering design*. Tata McGraw-Hill Education, 2011.

[26] N. Xydas, M. Bhagavat, and I. Kao, "Study of soft-finger contact mechanics using finite elements analysis and experiments," in *Robotics and Automation, 2000. Proceedings. ICRA'00. IEEE International Conference on*, vol. 3. IEEE, 2000, pp. 2179–2184.

[27] A. Reiterer, I. Burgert, G. Sinn, and S. Tschegg, "The radial reinforcement of the wood structure and its implication on mechanical and fracture mechanical properties—a comparison between two tree species," *Journal of Materials Science*, vol. 37, no. 5, pp. 935–940, 2002.

[28] S. Liu and S. Carpin, "Partial convex hull algorithms for efficient grasp quality evaluation," *Robotics and Autonomous Systems*, vol. 86, pp. 57–69, 2016.

[29] M. Abdeetedal and M. R. Kermani, "Development and grasp analysis of a sensorized underactuated finger," in *Intelligent Robots and Systems (IROS), 2017 IEEE/RSJ International Conference on*. IEEE, 2017, pp. 6331–6336.

[30] N. Kondo, K. Yata, M. Iida, T. Shiigi, M. Monta, M. Kurita, and H. Omori, "Development of an end-effector for a tomato cluster harvesting robot," *Engineering in Agriculture, Environment and Food*, vol. 3, no. 1, pp. 20–24, 2010.

[31] H. Wang, J. F. O'Brien, and R. Ramamoorthi, "Data-driven elastic models for cloth: modeling and measurement," in *ACM Transactions on Graphics (TOG)*, vol. 30, no. 4. ACM, 2011, p. 71.

[32] R. M. Rowell, *Handbook of wood chemistry and wood composites*. CRC press, 2012.